BACHELOR'S THESIS

Characterizing PneuFlex Actuator Deformations Using Liquid Metal Strain Sensors

Gabriel Donald Zöller

338616

Technische Informatik

examiners:

Prof. Oliver BROCK

Prof. Klaus-Robert MÜLLER

advisors:

Prof. Oliver BROCK

Vincent WALL

TECHNISCHE UNIVERSITÄT BERLIN

Fakultät Elektrotechnik und Informatik

Institut für Technische Informatik und Mikroelektronik

Robotics and Biology Laboratory

September 13, 2016

Eidesstattliche Versicherung

Hiermit erkläre ich, dass ich die vorliegende Arbeit selbstständig und eigenhändig sowie ohne unerlaubte fremde Hilfe und ausschließlich unter Verwendung der aufgeführten Quellen und Hilfsmittel angefertigt habe.

Berlin, den

.....
Unterschrift

Zusammenfassung

Weiche Roboterhände passen ihre Form ohne Zutun an Gegenstände und Oberflächen an und eignen sich deshalb besonders zum Greifen. Aber ihre Form kann auch Informationen über den Greiferfolg, Eigenschaften von Gegenständen und der Umgebung liefern. Diese Form zu messen erschwert sich eben durch diese Flexibilität, denn das weiche Material zeigt sehr komplexe Verformungen. Das Ziel dieser Arbeit ist, eine vereinfachte Formerkennung für den PneuFlex Aktuator der RBO Hand 2 zu ermöglichen. Dazu werden komplexe Verformungen als Kombination einfacherer Verformungen identifiziert, die wiederum durch Regressionsanalyse aus Dehnungssensordaten vorhergesagt werden können. Eine Anordnung von Dehnungssensoren wird mithilfe von Verformungsabschätzungen auf den Aktuator aufgebracht und durch ein Optimierungsverfahren auf die aussagekräftigsten Sensoren reduziert. Mit dieser optimierten Anordnung lassen sich diese elementaren Verformungen immer noch präzise vorhersagen, wodurch Aussagen über die tatsächliche Form des PneuFlex getroffen werden können.

Abstract

Soft, compliant robot hands passively adapt their shape to excel in grasping tasks. But their shape can also give insight into grasp quality, object properties and their environment. Recovering this shape is difficult because their soft material exhibits complex deformations when subjected to external force. This thesis aims to enable limited shape sensing of the PneuFlex actuator used for the soft RBO Hand 2. Complex actuator shapes are identified as combinations of simple deformations that are shown to be predictable from strain sensor readings using machine learning. A layout of strain sensors is created from strain estimations during these deformations and optimized to produce a reduced layout of sensors. This optimized layout is then shown to still accurately predict these deformations, giving insight into the shape of the PneuFlex actuator.

Contents

1 Introduction

The flexible shape of compliant actuators that form soft, pneumatic robot hands like the RBO Hand 2, is integral to their ability to reliably grasp objects and safely interface with their environment. Their soft material and pneumatic actuation allow passively adapting their shape to maximize contact area while grasping, as well as enduring impacts with little to no damage done to both the manipulater and the impactor.

But shape can also give information about object properties [1], grasp quality and the surroundings of the actuator [2]. Integrating proprioceptive shape sensors into the PneuFlex actuators that make up the RBO Hand 2 could enable these benefits.

Shape sensing of soft pneumatic actuators made from silicone rubber is impeded by two aspects: First, the high flexibility leads to highly complex deformations with very high, near infinite degrees of freedom, which are difficult to model and sense in all their degrees of freedom. Second, parts of the actuator stretch to up to 170 % of their original size and may bend in very sharp angles, requiring sensors as flexible as the actuator itself.

Strain sensor designs based on changing the resistance of a liquid metal conductor inside a strip of silicone rubber [3, 2] fit the PneuFlex actuator well. Being made from the same material, they exhibit the properties described in the second aspect above. Farrow and Correll [2] have used an actuator based on the same design as the PneuFlex actuator, equipped with a pressure sensor and a single liquid metal strain sensor (LMSS) to discern grasped objects and recognize contact with the environment.

The contribution of this thesis is a method to equip PneuFlex actuators with an optimized layout of multiple strain sensors able to measure simplified, task-oriented deformations, giving insight into the actuator's shape. These task-oriented deformations are derived by observing the RBO Hand 2 while grasping and exploiting

environmental constraints (3). The most common deformations occurring are divided into these constituting parts, called deformation modes. Sensor placement on the actuator is then motivated by estimating the strain induced by these deformation modes (4.1.2). A motion capturing system quantifies the deformation modes (4.1.5), allowing them to be predicted from strain sensor readings with a machine learning algorithm (4.1.6). The layout of sensors is then reduced to an optimized version that simplifies repeatable manufacturing (4.1.3) while retaining the accuracy of the full number of sensors.

While I apply this method to the PneuFlex actuator, it could be applied to other soft actuators operating with high amounts of stretch.

I first give an overview on related research regarding soft manipulators, appropriate sensing strategies and other work on sensorizing manipulators in 2. I further introduce the PneuFlex actuator, the RBO Hand 2 and deformation modes in 3. Afterwards, I explain the setup and execution of the experiment I conduct to test my method of finding an optimized layout of LMSSs on the PneuFlex actuator to predict deformation modes in 4. This experiment is evaluated, showing my method to work (5) and explaining its limitations and inspired future work (6).

2 Related Work

In this section, I give an overview on soft, compliant robot hands, research regarding shape sensing of soft manipulators, suitable sensor technologies and simulation of soft, pneumatic actuators.

Soft Manipulators Soft, underactuated manipulators have shown to provide robust grasping capabilities, inherent safety and lower manufacturing costs compared to mechanically more complex rigid or actively compliant robot hands.

In this work, I focus on the RBO Hand 2, a dexterous, soft robotic hand that uses PneuFlex actuators, pneumatic continuum actuators made from flexible silicone rubber [4].

Benefits of Sensors on Soft Robotics Sensing in soft manipulators can give insight into their surroundings, assess grasp quality and discern properties of grasped objects. This can improve grasping performance and make soft manipulators even safer.

Farrow and Correll [2] demonstrate the use of a liquid metal strain sensor (LMSS) and a pressure sensor on pneumatic actuator to distinguish objects and contact with the environment. Homberg et al. [1] show how to recognize objects with bend sensors inside soft actuators, forming a soft hand with three fingers with each containing one sensor. Each of these soft pneumatic actuators has at most one bend or strain sensor and may have a pressure sensor.

Kazemi et al. [5] use finger strain gauges to help their environmental constraints exploiting grasping by registering contact of the actuator tips with a surface.

There is research to use soft, compliant manipulators in minimally invasive surgery aiming to provide flexible manipulators that can navigate inside the body of a patient without injuring surrounding tissue by enabling tactile sensing [6] or the need

to move the point of entrance of the manipulators by enabling shape sensing with 3 conductive yarn sensors [7].

White et al. [8] describe triangular patches of silicone with 3 integrated LMSSs that allow sensing deformations of these patches with the intent to combine multiple patches to a thoroughly sensorized bigger patch of soft skin. This could enable shape sensing on arbitrary soft objects, although with an edge length of 10 cm they are too big to be applied to actuators roughly the size of human hands and the high amount of sensors might complicate the measuring setup, with each sensor requiring a measuring circuit.

The RBO Hand 2 is currently limited to a single pressure sensor. Equipping it with multiple proprioceptive sensors to gain insight into its shape could further improve its grasping capabilities.

Choice of Sensors for Soft Robotics After introducing the advantages of sensors in soft manipulators, I discuss the type of sensors used in soft robotics and evaluate why LMSSs are a suitable candidate for sensors on the PneuFlex actuator.

There are lots of sensors with possible application in/on soft robotics: Homberg et al. [1] use bend sensors embedded into the silicone rubber of the actuator. These bend sensors are of a fixed length and embedded into the non-stretching layer of the actuator.

Optical fiber Bragg grating sensors are used by Park et al. [9] on a compliant manipulator to measure forces occurring during grasping. While fiber Bragg grating sensors can measure multiple angles and have a small bending radius, they can not be stretched. On the PneuFlex actuator, this would confine them to the sides or insides of the actuator directly atop the fabric layer.

Apart from sensors integrated into the actuator, external means of shape sensing can also be used, like camera-based systems Oikonomidis et al. [10] or electromagnetic tracking systems Sun et al. [11] These systems need to be in line of sight or in close range to the actuators, so (self-)occlusion or a low range of action can impair the usefulness of these systems. These systems can also be enhanced by additionally using proprioceptive sensors like in Hsiao et al. [12].

There are also several designs of strain sensors that can match the flexibility of soft, pneumatic actuators.

3 conductive yarn sensors are used by Wurdemann et al. [7] to sense the shape of a small, soft continuum actuator and are stretched to up to 156 % of their original length.

Conductive Thermoplastic Material (CTPE) strain sensors can be extruded to form various shapes of and can stretch to up to 200 % of their original length [13]. Specialized mixing and extruding hardware is needed to produce them, though.

LMSSs are made from the same flexible silicone rubber as the PneuFlex actuator and a single sensor is by Farrow and Correll [2] on an actuator based on the same design as the PneuFlex. They do not require specialized hardware for manufacturing and match the design of the PneuFlex very well and are therefore a suitable choice of sensors for the PneuFlex actuator.

Strain Simulation In this work, I estimate strain from deformation modes and attach multiple promising sensors to sense deformations, even if the sensors might turn out redundant.

Research on simulating soft, pneumatic actuators is ongoing, but no existing system simulates dynamic use cases like grasps, yet. Polygerinos et al. [14] conduct finite element simulation of similar actuator, but only under inflation, deformations from external force are not (yet) simulated. Deimel and Brock [4, A] describe a model to calculate PneuFlex manufacturing parameters according to specific needs like a specific actuation range or pressure response, but also do not (yet) simulate deformations from external forces.

Research on automatically routing strain sensors according to strain simulations of dynamic deformations in simpler soft bodies made of a single material exists, like Culha et al. [13] use on 2 dimensional shapes and Bäecher et al. [15] use in a 2 dimensional plane in an action figure. This can not directly be applied to the PneuFlex actuator because it is more complicated, employing 3 different materials and a hollow body filled with air.

3 Deformation Complexity Reduction With Deformation Modes

In this chapter I give an overview on the PneuFlex actuator used for the RBO Hand 2 and argue why shape sensing could improve its performance. To enable shape sensing, I divide its complex deformations into 4 simpler deformations. I then estimate where these deformation modes induce high strain in the PneuFlex actuator to find candidate areas for possible strain sensor placement. When combined, the measured deformation modes can give insight into the actuators shape.

3.1 The PneuFlex Actuator and the Need for Shape Sensing

The PneuFlex actuator, as described by Deimel and Brock [16, 4] is a soft, pneumatic continuum actuator. Its soft, hollow shell is molded from flexible silicone rubber, then bonded to a bendable, but not stretchable layer of PET fabric and reinforced with a helical wrapping of thread [4, p.4]. This layer of fabric causes the PneuFlex to bend when inflated with air, while the thread helps to keep its expansion to the amount needed for bending [4, p. 4], as seen in figure 3.1. It is inflated and deflated by electric high-speed valves and monitored with a pressure sensor to prevent damaging the actuator from high internal pressure.

PneuFlex actuators allow the construction of the dexterous and passively compliant RBO Hand 2 [4], seen in figure 3.2. This soft robot hand can grasp in a wide variety of ways [4, p. 12] and achieves a firm grip on objects by passively

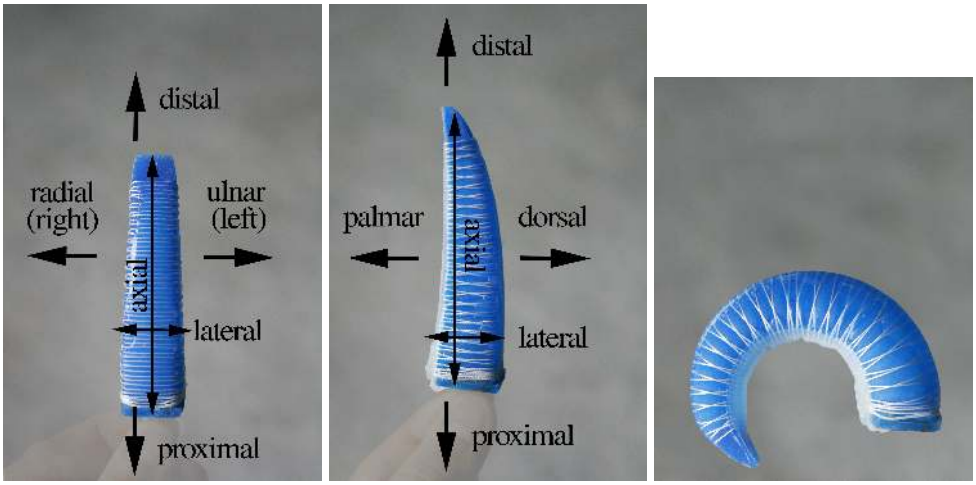

Figure 3.1: A PneuFlex actuator bending on inflation. The actuator's passive layer made of non-stretchable fabric keeps its length while the silicone shell extends. The thread-wrapping constrains the expansion of the actuator to the necessary amount to achieve bending. Anatomical terms of location are overlayed.[17]

adapting its shape. Its passive compliance also enables it to exploit environmental constraints like a wall or the edge of a table to improve its grasping performance [20, pp. 12-14].

But as I established in chapter 2, grasping performance of compliant manipulators can be improved with proprioceptive sensing [21]. Also, information about grasped objects [1] and grasp success [2, p. 2322] can be inferred from the actuator's shape. With parts of the PneuFlex actuators bending very sharply or stretching up to 170 % of their original length, sensor technologies just as flexible are needed.

In the following section, I propose a way to enable proprioceptive shape sensing in PneuFlex actuators.

3.2 Deformation Modes: Dividing Deformations to Enable Shape Sensing

The high flexibility of the PneuFlex actuator allows it to deform in complex ways with very high, near infinite degrees of freedom. While this is a prerequisite for the

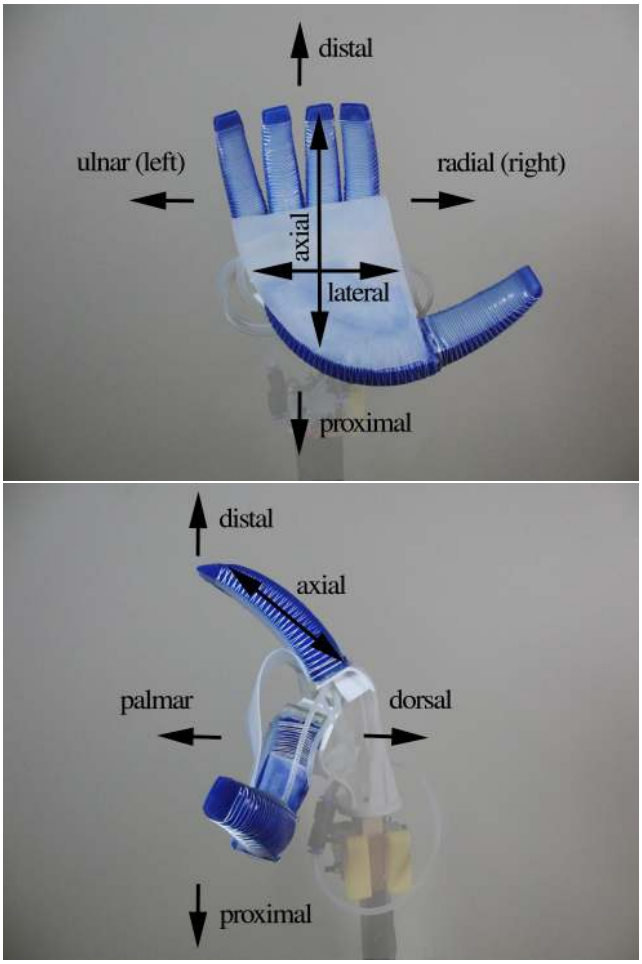

Figure 3.2: The RBO Hand 2, comprising 7 PneuFlex actuators: 4 as fingers, 1 as the thumb and 2 as the palm. Overlayed are the anatomical terms of location [18].[19]

passively compliant grasping abilities of the RBO Hand 2, it complicates sensing the shape of the actuators. Because each degree of freedom needs one independent sensor, a thorough sensorization of a PneuFlex actuator would need as many sensors as there are degrees of freedom.

A reduced amount of deformation degrees of freedom might sufficiently describe sensor shape to enable the benefits of sensing described in chapter 2. While reenacting grasps from the grasp taxonomy described by Feix et al. [22] and constraint exploitation by Eppner et al. [20, pp. 12-14] I observed that the most prominent deformations of the PneuFlex actuators are combinations of 4 simpler deformations. I

show a set of grasps executed with the RBO Hand 2 and how the occurring deformations can be divided. I then define the 4 deformation modes gathered from the division. Combining these deformation modes again should thus give insight into the shape of the actuator.

3.2.1 Grasps and Composite Deformation Modes

In this subsection, I divide PneuFlex actuator deformations into visible deformation modes.

Slide-to-Wall Grasp In the slide-to-wall grasp as described by Eppner et al. [20, p. 18] contact with the wall leads to lateral deformations, as seen in figure 3.3

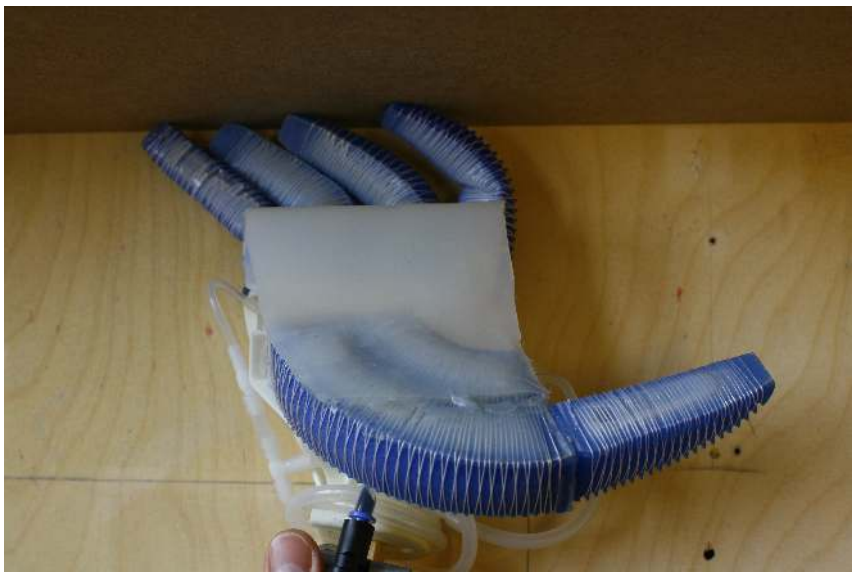

Figure 3.3: A slide to wall grasp leads to lateral deformations on contact with the wall. [17]

Medium Wrap Lifting Heavier Objects While a medium wrap grasp [22, No. 3] shows visible dorsal deflection, lifting the grasped object leads to lateral deflection combined with axial rotation, as seen in figure 3.4.

In general, lifting objects with the ulnar/radial axis parallel to the direction of gravity shows lateral deflection and/or axial rotation.

Power Disk Grasp With the power disk grasp as described by Feix et al. [22, Grasp No. 10], the actuators of the RBO Hand 2 show a very slight proximal/distal contact point, together with dorsal deflection, as seen in figure 3.5

3.2.2 Deformation Modes

Deformation modes are simple deformations of the PneuFlex actuator that have 1 degree of freedom. Their naming refers to the anatomical terms of location [18] as visualized in figure 3.2.

Palmar and Dorsal Deflection refers to deflection with (palmar) or against (dorsal) the direction of actuation of the PneuFlex actuator as seen in figure 3.6.

Lateral Deflection is a deflection perpendicular to the direction of actuation, as seen in figure 3.7. In an RBO Hand 2, this deformation mode would be named radial (towards the thumb) and ulnar (away from the thumb) deflection.

Axial Rotation is a rotational deformation around the proximal/distal axis of the actuator, as seen in figure 3.8.

Palmar Contact describes where contact occurs on the palmar PET fabric layer along the distal/proximal axis, as seen in figure 3.9.

3.3 Strain Estimation on the PneuFlex Actuator

As established in chapter 2, I use liquid metal strain sensors (LMSSs) to measure the extent of deformation modes of PneuFlex actuators. Strain sensors are obviously the most useful in areas where high strain occurs, so I need to find areas where deformation modes lead to strain in the PneuFlex actuator. But because simulating soft actuators in dynamic cases like external deformation is difficult [4, p. 8], computer aided strain estimation is not available and I visually estimate the strain induced by deformation modes.

In this section I explain how I found promising configurations of strain sensors on the PneuFlex actuator by estimating the strain induced during deformation.

Strain from Inflation According to the principle of function of the PneuFlex actuator, its soft silicone shell stretches while its fabric layer stays at the same length. This leads to strain in the whole silicone shell, but most prominently in the dorsal side of the actuator, opposite from the non-stretching fabric layer.

Strain from Deflection Deflection leads to strain from compression in the direction of deflection and to strain from stretching on the opposite side.

For palmar and dorsal deflection, most strain occurs on the dorsal and palmar side respectively, as seen in figure 3.6. The fabric layer on the palmar side does not compress like silicone parts do, but rather crumples slightly. But because the fabric layer is in direct contact with objects, LMSS can not be applied to it, because grasping would pinch off sensors and lead to invalid measurements. This leaves the dorsal side of the actuator to place a strain sensor that measures strain from palmar deflection and compression from dorsal deflection.

For lateral deflection, the opposite sides are both made from silicone, so stretch and compression occur on both sides, as seen in figure 3.7. So both lateral sides of the PneuFlex are promising areas for sensor application.

Strain from Axial Rotation Axial rotation twists PneuFlex actuator, leading to strain wrapping helically around the actuator in the direction of the rotation, as visualized in figure 3.8. Likewise, strain sensors wrapped around the PneuFlex helically in both directions should be able to measure this deformation mode.

Strain from Contact on the Palmar Fabric Layer A sharp contact on the fabric layer leads to the parts of the actuator before and after the contact point to stretch differently, as seen in figure 3.9.

This motivates multiple sensors of different length along the dorsal side of the actuator. Because this deformation was actually visible only in a few cases (see subsection 3.2.1), I decided to integrate sensors of only two lengths.

3.4 Conclusion

I introduced the PneuFlex actuator as the constituting parts of the soft RBO Hand 2. I described divisions of prominent PneuFlex deformations resulting from grasping tasks into 4 simpler deformations called deformation modes. To allow measuring of deformation modes with strain sensors, I estimated where deformations would induce high strain on the actuator.

Figure 3.4: Grasping a heavy object with a medium wrap induces dorsal deflection. Trying to lift it induces axial rotation and lateral deflection. [17]

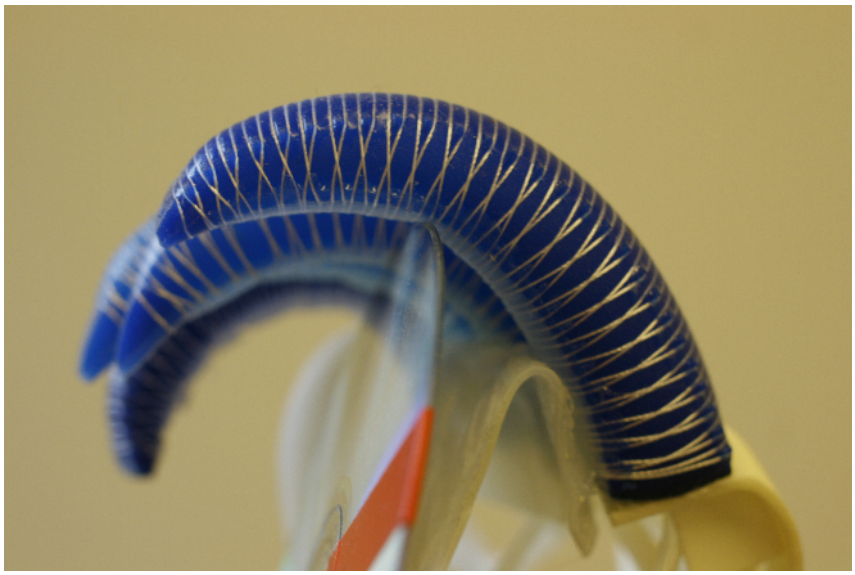

Figure 3.5: A power disc grasp shows obvious dorsal deflection and a proximal/distal contact point. [17]

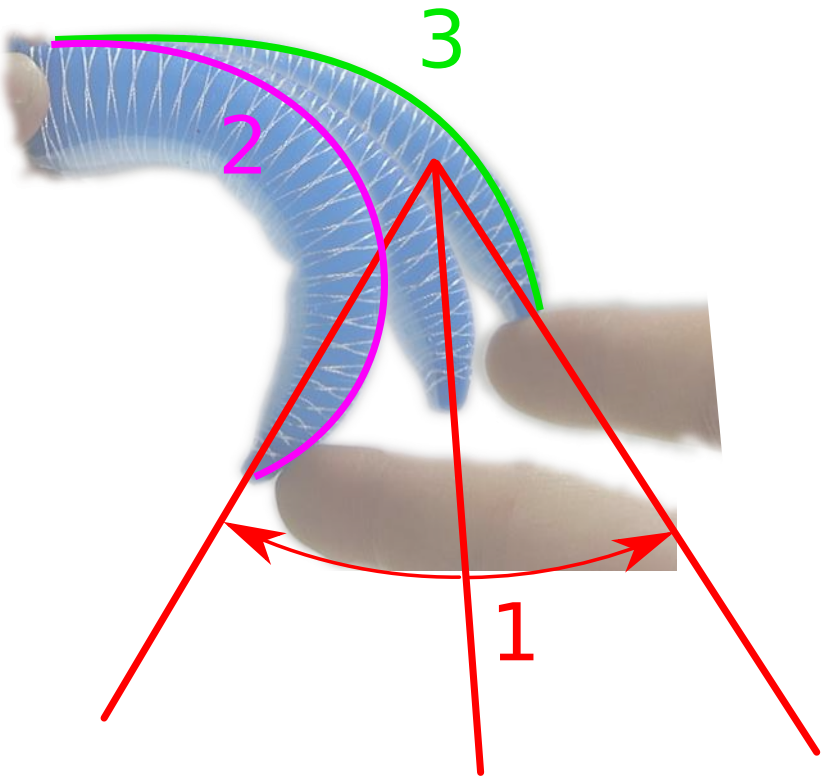

Figure 3.6: Palmar and dorsal deflection respectively occur with or against the direction of actuation of the PneuFlex actuator. Palmar deflection leads to stretching on the dorsal side (2) and to crumpling in the fabric layer. Dorsal deflection leads to compression on the dorsal side (3). The fabric layer does not stretch. High strain occurs thus on the dorsal side. This deformation is parametrized by the angle (1).

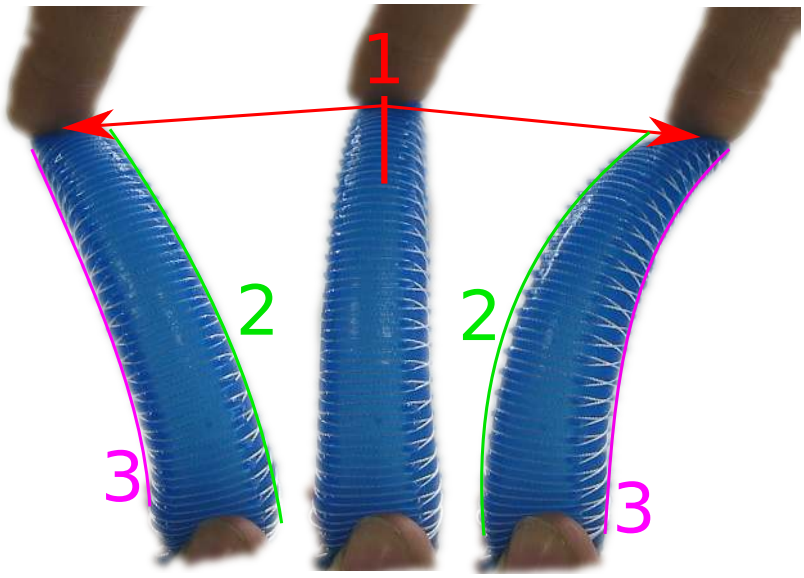

Figure 3.7: Lateral deflection occurs perpendicular to the direction of actuation of the PneuFlex actuator. The lateral sides of the PneuFlex stretch and compress on lateral deflection. Compression occurs in the side in the direction of the deflection (3) and stretching in the opposite side (2). This deformation is parametrized by the distance (1).

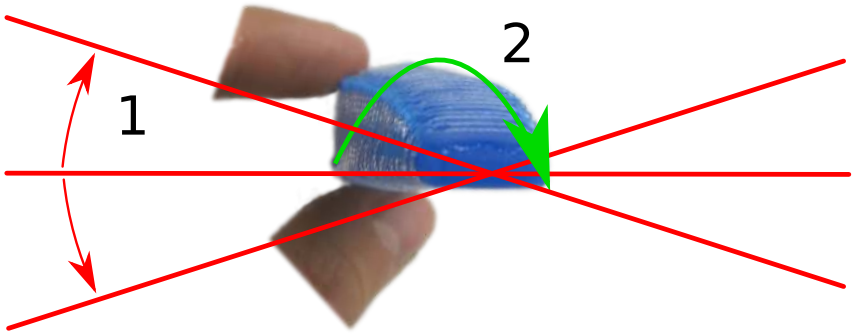

Figure 3.8: Axial rotation refers to the rotation around the proximal/distal axis of the PneuFlex actuator. Strain occurs in a spiral around the actuator as indicated by (2). This deformation is parametrized by the angle (1).

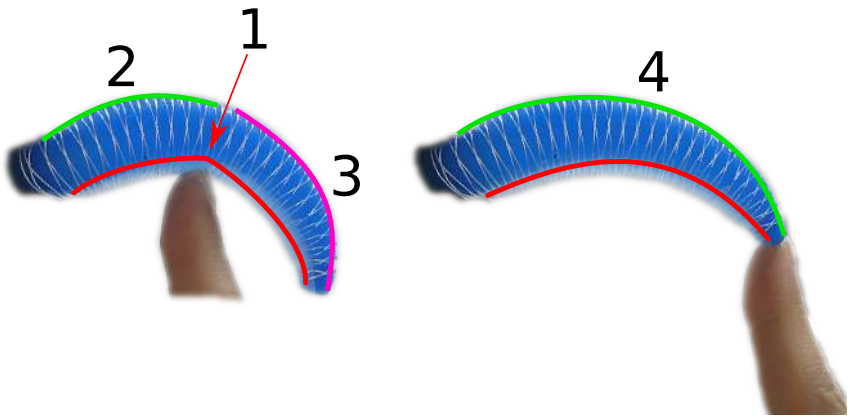

Figure 3.9: Palmar contact refers to where on the fabric layer of the PneuFlex a sharp contact occurs. Sharp contact on the fabric layer (1) sections the PneuFlex into two parts bending with different angles (2 and 3). Different amounts of strain occur before and after the point.

4 Experimental Setup and Execution

After introducing deformation modes and estimations where they induce high strain in chapter 3, I describe the experiment I conduct to test if deformation modes can be predicted from liquid metal strain sensor (LMSS) data. In this experiment I manually bend the PneuFlex actuator into singular or combined deformation modes (4.2) while recording sensor data (4.1.4) and positional information about the actuator. The positional information is then converted into the extent of deformation modes (4.1.5). I expect to be able to quantitatively predict deformation modes from strain sensor readings and find a reduced set of sensors that allows this prediction with similar accuracy. For the prediction, I train a machine learning algorithm on the gathered data and gradually reduce the amount of sensors used as the prediction input to find a suitable reduced set of sensors (4.1.6). I analyze and determine the success of the experiment on the basis of error metrics in chapter 5.

4.1 Setup

This section describes the hardware and software setup of the experiment. I first introduce LMSSs, explaining their properties and the manufacturing process in subsection 4.1.1. In subsection 4.1.2, I compile a set of sensors that is tested in the experiment, based on the strain estimations from section 3.3. Strain and pressure sensor data acquisition, cleaning and scaling is described in subsection 4.1.4 and the setup to gather positional data and to convert it into deformation modes in subsection 4.1.5. The machine learning setup to predict deformation modes from sensor data and to find a reduced set of sensors is explained in subsection 4.1.6. In 4.1.3 I describe the reasoning behind and the manufacturing of a sensor layout arranged in

a single sheet of silicone. This reduced layout is then tested in a new round of the experiment to test the results of the previous one.

4.1.1 Liquid Metal Strain Sensors

The liquid metal strain sensors (LMSSs) I use on the PneuFlex are a design of resistive strain sensors described by Farrow and Correll [2, pp. 2319-2320]. They consist of a silicone tube with a diameter of 0.12 mm encased in a thin layer of silicone and filled with a eutectic gallium-indium-tin alloy that is liquid down to $-19\,°C$ [23] and is electrically conductive. When the sensor is stretched, the tube elongates and its diameter decreases, which both raise the electrical resistance of the liquid metal. The resistance of a single sensor is about $0.9\,\Omega$ unstretched and $1.4\,\Omega$ fully stretched. But when the sensor is pinched and the tube closes off, the electric conductivity is interrupted. For this reason, LMSSs can not be used on the palmar side of PneuFlex actuators because grasping objects would lead to pinch-off.

Manufacturing A piece of silicone tube with an inner diameter of 0.12 mm is stretched out in a U-shape at the bottom of a mold with its ends fastened at the edges of the mold. A 1 mm layer of silicone is filled into the mold, encasing, but not filling the tube. After being lifted from the mold and roughly cut to shape, the liquid metal is injected into one end of the silicone tube. Insulated copper wire with a diameter of 0.25 mm is stripped and inserted into the metal-filled tube. Pieces of mesh are attached to both ends of the U. “On the distal end the mesh prevents the tube from stretching at the tip, keeping the active area of the sensor confined to the straight part.” ([2, p. 2320]) On the proximal end, the mesh overhangs the sheet of silicone by about 2 cm. While the mesh on the silicone relieves strain [2, p. 2320] and hinders the inserted wire from piercing the silicone, the overhanging mesh is attached to the wire to prevent it from being pulled out.

4.1.2 Strain Sensor Placement

In chapter 3 I introduce deformation modes and the corresponding areas of high strain on the PneuFlex. I use these strain estimations to motivate the placement of strain sensors and attach them to the actuator with a silicone adhesive.

Palmar and Dorsal Deflection lead to high strain in the dorsal side of the actuator. Because the palmar side of the finger contains the fabric layer, doesn't stretch and in direct contact with objects, it is an unsuitable area for a LMSS. I thus attach a LMSS across the full length of the dorsal side of the actuator.

Lateral Deflection leads to high strain on the lateral sides of the actuator. I attach a full length sensor on each side of the actuator. This might prove to be redundant because one sensor could be sufficient to measure deflection in both directions. But because the lateral sides also stretch and compress on palmar and dorsal deflection, albeit less than the dorsal side, two sensors might prove advantageous in distinguishing the two deformation modes.

Axial Rotation leads to strain helically wrapping around the actuator. I decide to attach 5 sensors to the actuator to measure this deformation, as seen in figure **??**, based on 2 different arguments:

1. I attach 2 strain sensors reaching from one side of the proximal end to the opposite side on the distal end, because axial rotation can have two directions, see sensors 6 and 7 in figure 4.2. Again, as with lateral deflection, this might prove redundant.

2. I wrap 3 sensors in a row fully around the PneuFlex, see sensors 8, 9 and 10 in figure 4.2. While this goes against not sensorizing the fabric layer, the sensors might be more informative when they fully wrap around the actuator. Should these sensors prove to be more useful than the other set, a similar sensor design might be found that does not cross the fabric layer, but still provides more than one loop.

Palmar Contact Sharp contact on the fabric layer splits the actuator into 2 sections bending differently. Each section needs its own LMSS. The longer sections are already sensorized laterally and dorsally. To measure the shorter sections, sensors of half the length of the other sensors are applied laterally and dorsally. While this also means half-length sensors will be under strain from palmar/dorsal and lat-

eral deflection, the combination of half-length and full-length sensor should enable measuring palmar contact.

Final Layout As seen in figures 4.1 and 4.2, the actuator used in the experiment has 10 LMSSs applied:

1. 1 sensor along the full length of the dorsal side.
2. 2 sensors along the full length of the lateral sides.
3. 1 sensor along half the length of the dorsal side.
4. 1 sensor along half the length of a lateral side.
5. 2 full-length sensors in an X-shape atop the actuator.
6. 3 sensors in a row, each wrapping around the actuator once.

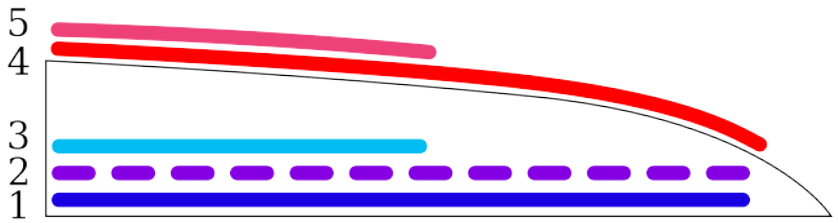

Figure 4.1: 1 sensor along the full length of the dorsal side (4). 2 sensors along the full length of the lateral sides (1, 2). 1 sensor along half the length of the dorsal side (5). 1 sensor along half the length of a lateral side (3). [17]

4.1.3 Arranging Sensors in One Sheet of Silicone

This section describes why and how I arrange the set of sensors resulting from the reduction in one sheet of silicone. On the actuator used for the experiment, the sensors are attached on top of each other and reduced the flexibility of the actuator. To keep this loss of flexibility to a minimum, the set of sensors derived from the experiment is arranged in a single layer of silicone. This also helps to attach the

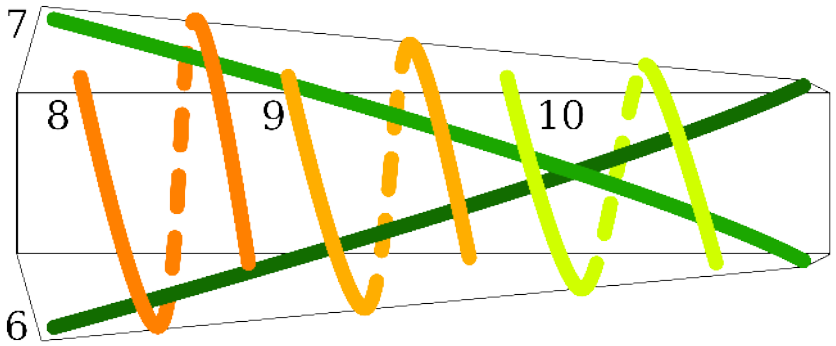

Figure 4.2: 2 full-length sensors in an X-shape atop the actuator (6, 7). 3 sensors in a row, each wrapping around the actuator once (8, 9, 10). [17]

sensors to the finger in a repeatable manner, because sensor positions vary less than when attaching sensors one after another. On the other hand, arranging a higher amount of sensors in a single sheet of silicone renders the manufacturing process more error prone, so finding a reduced but informative set of sensors is desirable.

To design this layout, I flatten an unused PneuFlex shell and align the 4 sensors resulting from the sensor reduction on it, as seen in figure 4.3.

4.1.4 Gathering and Cleaning Sensor Data

Here I describe how I measure the strain and pressure sensors attached to the PneuFlex actuator and the post-processing I apply to these measurements.

Measuring Sensors I measure the strain sensors and pressure sensor for the PneuFlex with a LabJack U6 USB data acquisition (DAQ) device.

The NXP MPX4250 pressure sensor is an integrated device and measured according to its specification [24].

The LMSSs on the PneuFlex are measured using a simple voltage divider circuit with a resistor of 156 Ω to set their voltage at roughly 30 mV. The LabJack DAQ samples at a rate of 20 Hz, a resolution of 16 bit and an amplification factor of 1000.

Zeroing and Scaling Because LMSSs have a very small resistance in the range of 0.8 Ω to 1.4 Ω, they carry a few disadvantages. Sensors are subject to offsetting

while the relative amplitude stays the same. This might be due to changing contact resistance when the sensor wires are touched or otherwise disturbed. To mitigate offsetting, sensor readings have to be zeroed while the actuator is in a neutral position before use and future designs should use more robust electrical terminals like wider pin headers.

While not strictly necessary for the regression algorithms used in 4.1.6, sensor data is also rescaled. This is intended to mitigate sensor drift, which I suspect to also occur in addition to the offsetting described above, but this suspicion will turn out to be false. For this, a calibration movement is executed at the beginning of a new recording and sensor readings are rescaled to an interval of $[0, 1]$, as seen in figure **??**. Later sensor readings are scaled with the same parameters, but might be greater than 1 or less than 0. They are then offset so their undisturbed values sit at 0.

Another problem stemming from the low resistance is quantization noise, as seen in figure 4.4. To reduce this noise, the readings are filtered with a second order Butterworth lowpass filter with a cutoff frequency of 2 Hz.

4.1.5 Recording and Extracting Deformation Modes from Motion Capture

A quantitative description of deformation modes is needed to allow their prediction from LMSS-data. Deformation modes can be quantified on a 1-dimensional scale because they have 1 degree of freedom. I calculate quantified deformation modes from the positions of motion capturing markers attached to the PneuFlex actuator. I succeed in calculating the palmar, dorsal and lateral deflection and the axial rotation of the PneuFlex, but fail to calculate the contact point on the fabric layer.

Motion Capturing System The motion capturing system consists of a set of 10 cameras and infrared light (IR) emitters observing and illuminating a volume from different viewpoints. By determining their relative positions, it is possible to localize IR-reflective markers within the observed volume very accurately, with precision of below 1 mm and a sampling rate of 100 Hz.

The resulting localization data consists of timestamped X-, Y- and Z-coordinates of each marker.

The system can continuously identify sets of markers on rigid structures, though this identification is not always correct. Wrongly identified markers are manually corrected and jitter is reduced by smoothing with a Butterworth low pass filter with a cutoff frequency of 15 Hz.

Markers missing due to occlusion during the experiment are rare and of short duration because the volume is thoroughly covered by the cameras. If markers are lost during a static part of the experiment, like the actuator being held in a position, they are estimated between the last and next known positions. If markers are lost during a movement of the actuator, the experiment is aborted and repeated.

Motion Capturing Marker Placement To quantify deformation modes, I need to localize different parts of the actuator.

The 3 markers at the base on which the actuator is mounted are used as reference in calculations.

Deflection and axial rotation can be inferred from the position and orientation of the tip. For this, a rigid, L-shaped piece of plastic is attached to the tip and populated with spherical motion capturing markers at the ends and at the corner, as seen in red in figure 4.5

I plan to infer the palmar contact point position from a set of 8 markers applied on sticks at the lateral side of the actuator, as seen in purple in figure 4.5

Because the other deformation modes can be calculated with a single transformation and the goal of the experiment – that deformation modes can be predicted from LMSS data and an accurate, reduced set of sensors can be found – can already be achieved with the other 3 deformation modes, I continue the evaluation without the palmar contact point.

Calculating Deflection and Rotation Palmar, dorsal and lateral deflection and axial rotation are calculated from the position and orientation of the markers on the tip of the actuator using the following transformation:

In the beginning, all marker coordinates are in a coordinate system defined within the volume observed by the motion capturing system. The markers at the mount form an orthonormal base B with the following axes:

- The X-axis pointing from the mount-corner marker to the mount-side marker
- The Y-axis pointing from the mount-corner marker to the mount-bottom marker
- The Z-axis perpendicular to X- and Y-axis

Each position of the L-markers is then converted into base B.

1. Lateral deflection is parametrized by the X-coordinate of the L-origin.
2. Because palmar/dorsal deflection and axial rotation are parametrized as rotations of the L-frame relative to a reference, the L is angled and needs to be corrected to allow calculation of the palmar/dorsal deflection and axial rotation. For this, a correct base C is created from the unit vectors of the mount base. A transformation matrix from the angled L base into the correct base is calculated and used to transform all L coordinates.
3. At a neutral position of the actuator, a position of the L-markers is used as a reference to which the deformations are calculated.
4. A transformation matrix from the current corrected L to the reference L is calculated. This matrix contains the rotational transformations used to quantify 2 of the 3 deformation modes: Palmar and dorsal deflection and axial rotation. It is first transformed into a homogeneous transformation and then into rotations around ZYX-axes. Palmar/dorsal is the rotation around Z-axis, as seen in figure 3.6. Axial rotation is the rotation around X-axis, as seen in figure 3.8. Lateral deflection is X-axis of uncorrected L in base coordinates, as seen in figure 3.7.

4.1.6 Deformation Mode Estimation and Layout Reduction

This section describes the machine learning setup I use to predict deformation modes from sensor data and find a reduced set of sensors.

Regression I use linear and polynomial regression from the scikit-learn library [25] with leave-one-out cross-validation to get a prediction model. The 11 sensor readings described in subsection 4.1.4 are used as training data and the 3 deformation modes are used as target data for a regression algorithm. As described in 4.1.5, contact on the fabric layer is not successfully parametrized and is not used in the regression. Of the 5 recorded runs of the experiment, I randomly choose 1 run as a test set. 11 different models are trained on the 4 remaining runs in a leave-one-out cross-validation scheme. These 11 models are linear regression and 2-6 degree polynomial regression, once including all terms and once including only interaction terms. The average of the 4 validation mean squared errors (MSEs) is used as a metric to rank each regression algorithm.

Sensor Selection by Recursive Feature Elimination Reducing the amount of sensors used on a PneuFlex allows faster and more consistent manufacturing, as argued in section 4.1.3. It also reduces the amount of DAC-inputs needed, slightly simplifying the measuring setup. I determine a reduced layout of sensors by using the following elimination scheme: I use a leave-one-out-scheme on the n training vectors with $n \in [11,2]$. The n resulting sets of $n-1$ training vectors are trained with the different regression algorithms. For each algorithm, the set of $n-1$ sensors with the lowest average validation error is used in the next round of the elimination scheme with $n-1$ sets of $n-2$ training vectors, thereby removing the least significant sensor in each round. Afterwards, the combination of regression algorithm and set of sensors with the lowest validation error is selected.

4.2 Execution

In this section I describe how I carry out the experiment to test if PneuFlex deformation modes can be predicted from LMSS readings. The PneuFlex actuator with attached strain and pressure sensors is placed inside the volume of the motion capturing system and attached to a compressor. The actuator is then inflated to 1 of 5 pressure levels, called steps, the order of which is chosen at random. 5 steps of different pressure levels are combined to a run and 5 runs are recorded. During each step, after recording is started, a calibration movement is executed and I be-

gin applying deformation modes. The actuator is then deflated and the recording stopped.

Pressure Steps The inflation valve is opened for fixed amounts of time to reach 1 of 5 pressure levels. Because the supply pressure for the actuator is fixed to 2 bar, a fixed inflation time leads to the same pressure within the actuator. To cover the range of actuation of the PneuFlex, I choose the following 5 pressure steps to which the actuator is inflated: 1 step with the actuator deflated, 1 step at the maximum pressure before damaging the actuator, and 3 steps in between.

For the actuator with 10 LMSS attached (see 4.1.2), this results in 0 bar, 0 bar, 0 bar, 0 bar, 0 bar and 0 bar.

For the actuator with the reduced single-plane LMSS layout (see 4.1.3, this results in 0 bar, 0 bar, 0 bar, 0 bar, 0 bar and 0 bar.

Step and Run Randomization I opt to conduct 5 runs, because this allows for a 4-1 split for 4-fold cross-validation with 1 test set, as discussed in 4.1.6. I record each of the 5 pressure steps 5 times in a randomly assigned order and combine them to 5 runs, with each run containing every pressure step once. This randomization mitigates progressive changes that might occur in the setup, like slight decalibration of the motion capturing setup, or how I apply deformation modes.

Calibration Movement Before each step, the actuator is inflated to the highest pressure step and deflated again before inflating to the current pressure step. This is called a calibration movement, because it allows consistent scaling as described in section 4.1.4 and is visible in both the sensor recording and the motion capture, thereby simplifying identification and correction of temporal misalignment.

Applying Deformation Modes The experiment is directly derived from the deformation mode observations as described in chapter 3. I manually apply deformations at the tip of the actuator and at different pressure levels to cover most of the deformation space. After inflating the actuator, I manually bend the PneuFlex into deformation modes.

- I deflect the actuator in palmar, dorsal and both lateral directions.

- I rotate the actuator axially.
- I describe circles of different radius, thereby combining palmar/dorsal and lateral deflection.
- I deflect the actuator laterally in a way that leads to both lateral deflection and axial rotation, as it was observed when lifting heavier objects, and then deflect the actuator in palmar/dorsal direction, combining all 3 deformation modes.

I furthermore apply contact at 2 different points on the fabric layer in another set of runs, but as described in section 4.1.5, I do not successfully evaluate these runs.

4.3 Summary

In this section, I described the setup and execution for my experiment to test if PneuFlex deformation modes can be inferred from liquid metal strain sensor (LMSS) readings. I introduced liquid metal strain sensor (LMSS) as soft, resistive strain sensors that fit the design of the PneuFlex actuator well. Multiple sensors are placed on the actuator to cover the strain induced by deformation mode application. They are measured using a LabJack USB data acquisition (DAQ) and post-processed to mitigate averse effects from contact resistance. Motion capturing markers are applied to the actuator to acquire location and orientation of its tip, from which quantified deformation modes are calculated. Inside the motion capturing volume, I manually apply deformation modes at different pressure levels to the actuator to cover most of the deformation space of the modes. With the resulting data, regression algorithms are trained and evaluated on their ability to predict deformation modes from sensor data. A reduced set of sensors is found through a recursive elimination scheme and manufactured in a single sheet of silicone. The experiment is repeated with this new layout to validate the results of the reduction phase.

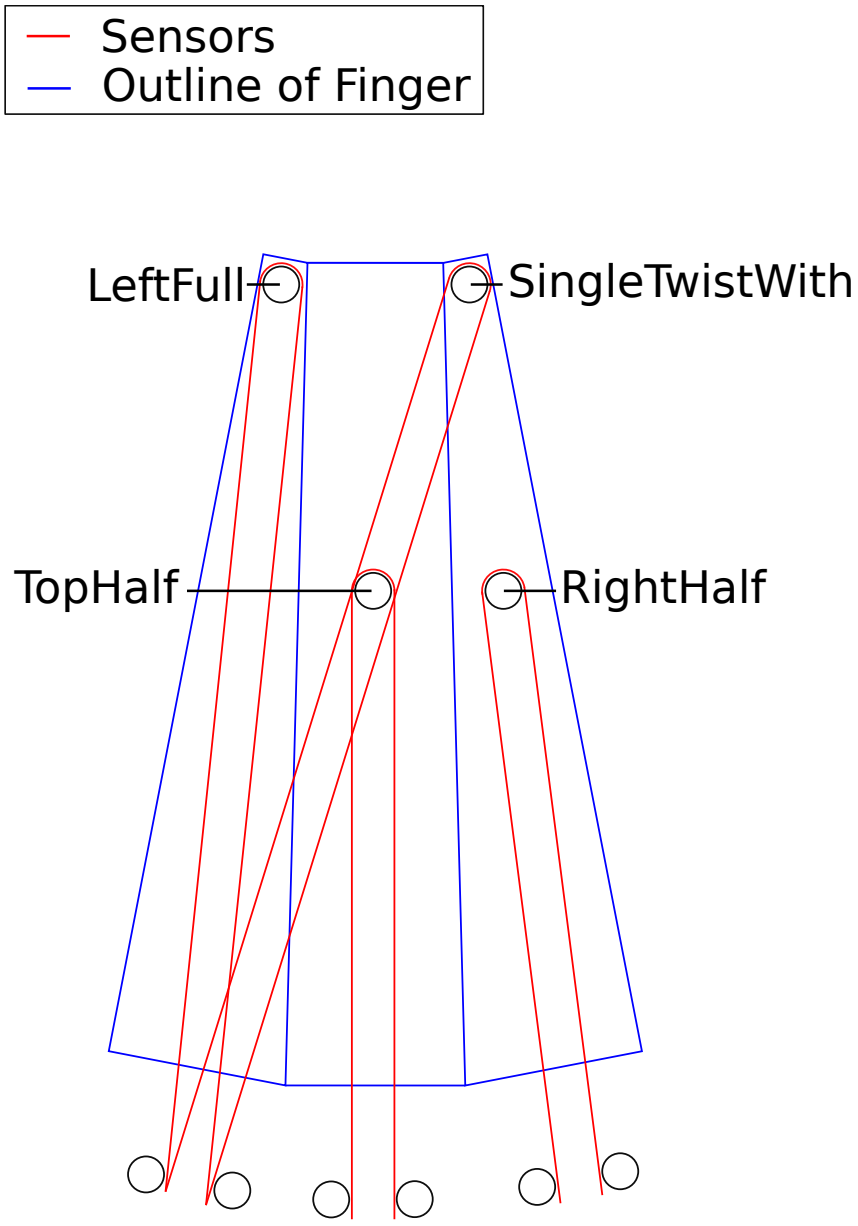

Figure 4.3: Schematic of reduced layout arranged in single plane.

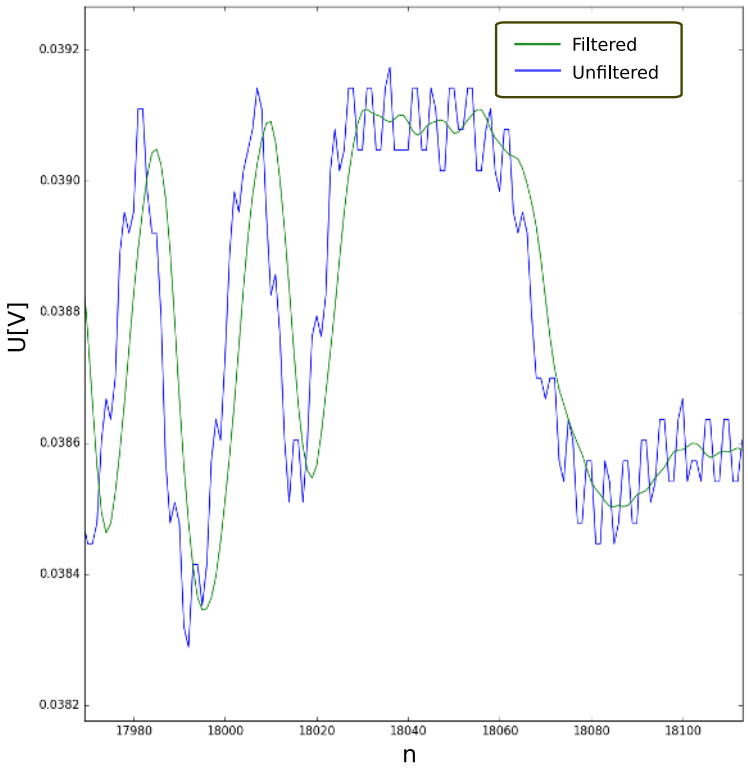

Figure 4.4: Quantization noise unfiltered and filtered.

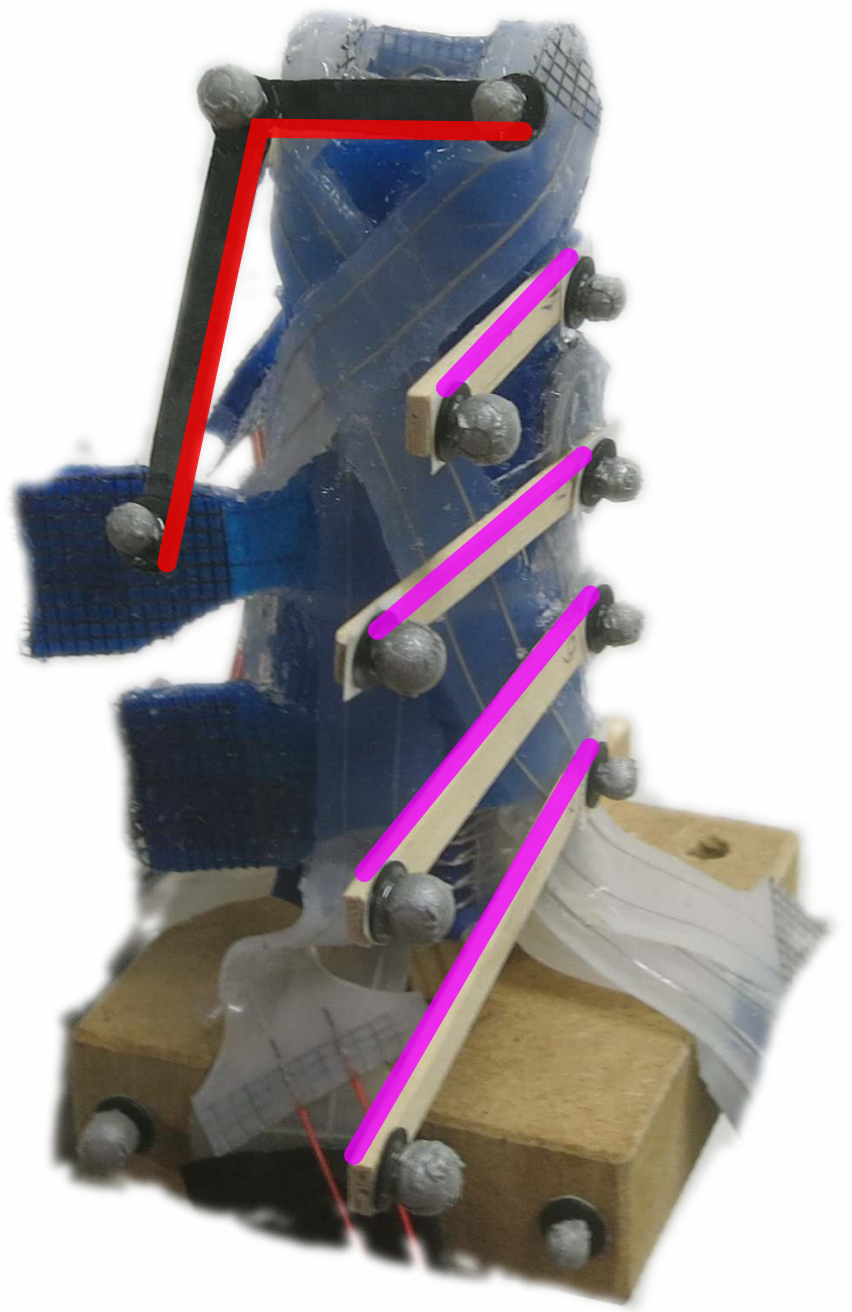

Figure 4.5: The PneuFlex actuator with attached motion capturing markers. The L-shaped markerset, highlighted in red, enables calculation of deflection and axial rotation. The markerset highlighted in purple should have enabled calculation of the contact point on the fabric layer, but this deformation mode was dropped for the experiment, as described in 4.1.5.

5 Evaluation

In this chapter, I evaluate the experiment described in chapter 4. I show that strain sensors placement motivated by strain estimations on the PneuFlex actuator allows prediction of PneuFlex deformation modes, even with a reduced set of sensors.

I first give a short overview over the methods and metrics used to generate and score the results, and the layouts under test.

Then I present how well PneuFlex deformation modes can be predicted and show results of the sensor reduction.

Afterwards, I discuss the prediction and reduction results.

5.1 Methods and Metrics

I evaluate the prediction of the following 3 layouts of liquid metal strain sensors (LMSSs): The full set of 10 LMSSs and the reduced set of 4 LMSSs on the PneuFlex used in the initial experiment, and the set of 4 LMSSs manufactured in a single plane after the reduced layout was determined.

As introduced in section 4.1.6, I train linear and 2-6 degree polynomial regression on LMSS readings to predict PneuFlex deformation modes. Of the 5 runs gathered in the experiment, 1 run is randomly chosen as a test set and only used in the final evaluation. The other 4 runs are fit using a leave-one-out cross-validation scheme.

I compare the mean squared error (MSE) of linear and 2-6 degree polynomial regression to find the most suitable algorithm.

For the best faring algorithm, I present MSE and coefficient of determination (R^2) scores over training, validation and test sets.

For the full and reduced layouts of the actuator used for the initial experiment, I compare real and predicted deformation modes from the test set run. I explain

and discuss different parts of this prediction to give a better overview over how well deformation modes are predicted.

For the sensor elimination, I show the development of the MSE during reduction as a heatmap.

MSE penalizes prediction errors quadratically, so larger errors more heavily impact the score than smaller errors. It is used as a metric to score different sensor selections against each other in the reduction phase.

R^2 is the relation between the variance correctly predicted and the total variance. A high R^2 implies a small error-range compared to the overall range of actuation. R^2 is also a comparison of a predictor to the naïve constant predictor, which has an R^2 of 0. So each predictor with $R^2 > 0$ is better, each with an $R^2 < 0$ is worse than a constant predictor.

5.2 Presentation

In this section, I present how well the full and reduced layouts of LMSSs allow the prediction of deformation modes of the PneuFlex actuator and how sensors are eliminated to find an informative, but reduced sensor layout.

5.2.1 Predicting PneuFlex Deformation Modes

In this section, I show the results of deformation mode prediction with 3 different layouts: The full set of 10 LMSSs and the reduced set of 4 LMSSs on the actuator from the experiment, and the single-plane-layout of 4 LMSSs. For each layout, a validation curve is generated, showing the training and validation errors over different degrees of linear and polynomial regression. Overall training-, validation- and test-scores of the optimal regression algorithm for each layout are presented. The deformation modes of 1 step of the test set are compared with predictions from the full and reduced layouts.

Validation Curves and Overall Scores Figure 5.1 shows the training and validation errors over the different regression algorithms for each of the layouts.

Figure 5.1a for 10 sensors, figure 5.1b for 4 sensors on the actuator used in the first experiment and 5.1c for the actuator with the single-plane-layout applied.

Figure 5.1a has its minimum validation error of 17.64 at degree 2 with interaction terms only, 5.1b an error of 12.16 at degree 3 with all terms and 5.1c an error of 17.38 at degree 4 with interaction terms only. The training error falls with higher degrees of regression, while the validation error rises slightly.

Prediction Comparison Figure 5.2 shows 1 step of the test set run, with deformation modes applied during the experiment in blue, deformation modes predicted from 10 LMSSs in green and from 4 LMSSs in red. In the subfigures, sections of interest are marked: It shows the calibration movement, palmar/dorsal and lateral deflection, axial rotation, a circle motion, inflation, deflation and the movement combining all 3 deformation modes.

The small difference between the predictions and the test data shows that the deformation modes are predicted very well in this step.

?? shows the whole test set, with one step suffering from bad prediction, probably due to a change in sensor contact resistance.

5.2.2 Finding a Reduced Set of Sensors

The elimination scheme, as described in 4.1.6, removes the sensors with the least significance. In this section, I first present a heatmap of sensor significance.

Figure 5.4 shows the effect of sensors removed from the current layout on the MSE. Each combination of regression algorithm (X-axis) and removed sensor (Y-axis) is assigned a square on the heatmap. The heatmap signifies a lower MSE with blue, a higher MSE with red. The sensor whose removal leads to the lowest MSE is marked with ”best” and removed for the next step. Removal of sensors like dorsal half-length significantly raises the MSE and is considered very important throughout the reduction.

Figure 5.5 shows the training (blue) and validation (green) errors over the layout produced by each reduction step. The minimum overall validation error occurs at the layout with 4 sensors: Lateral right half-length, dorsal half-length, lateral left full-length and left proximal to right distal.

5.3 Discussion

Through my experiment I want to test if strain estimations can motivate placement of sensors to characterize PneuFlex deformation modes.

The results presented in 5.2.1 show that this is possible.

As seen in 5.2 and corroborated by the R^2 value of $0.92 - 0.99$, deformation modes are predicted within a margin of error that is small compared to the full range of the deformation mode. Reduced layouts with an R^2 value of $0.95 - 0.98$ are also able to predict deformation modes within a similar margin.

In section 4.1.2, I motivated the placement of sensors according to the strain estimates from section 3.3. For each deformation mode, I described multiple possible placements of sensors, arguing that other deformation modes also induce strain in these positions.

The final layout of 4 sensors – lateral right half-length, dorsal half-length, lateral left full-length and left proximal to right distal – contains sensors motivated by each of the deformation modes, including the palmar contact point: While the sensors of half-length are motivated by the palmar contact point, they are similar to the full-length sensors motivated by the deflection deformations. The full-length sensor on the left side is motivated by lateral deflection and the sensor placed across the actuator from left to right by axial rotation. This shows that strain estimation and placing sensors accordingly, produces informative sensor placements to predict deformation modes. This is corroborated further by the heatmap showing the sensor's importance for the respective deformations.

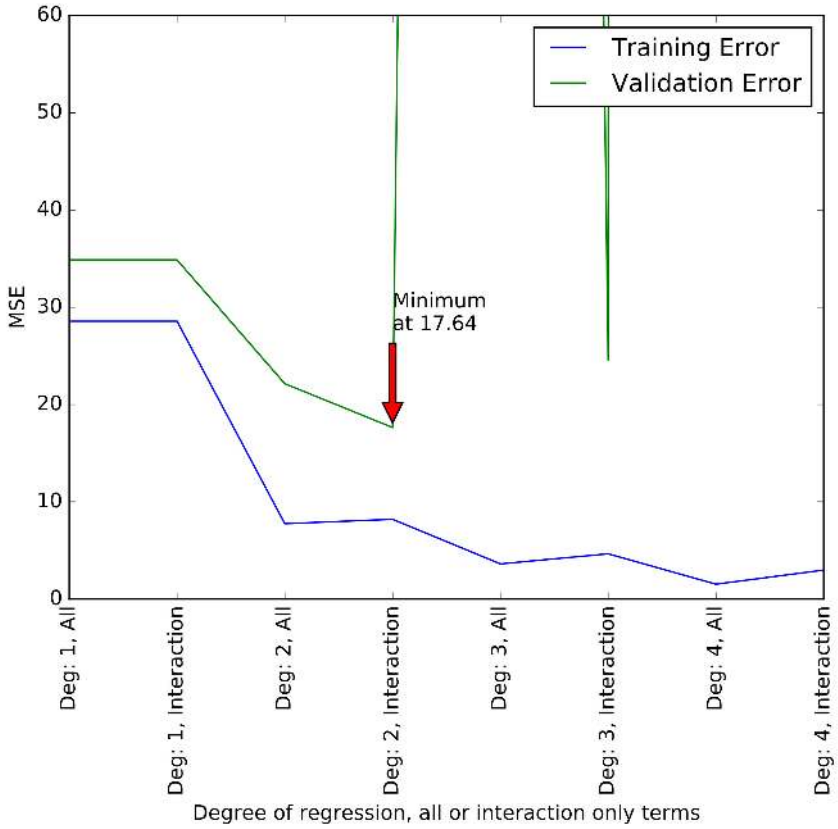

(a) Full set, 10 sensors plus pressure. Some models are overfitting and lead to very high MSEs.

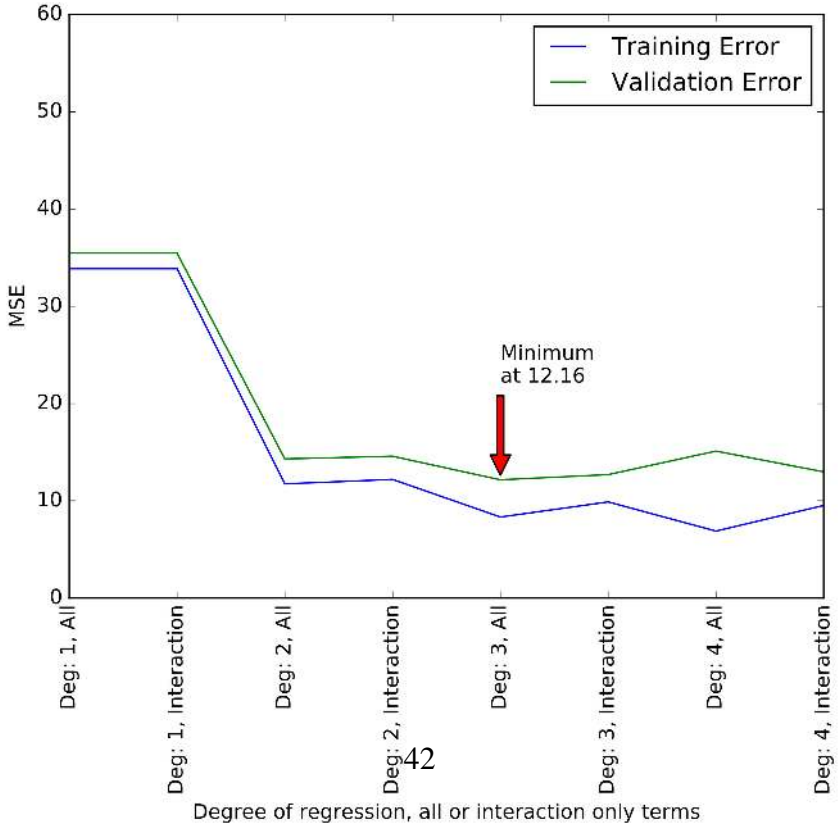

(b) Reduced set, 4 sensors plus pressure

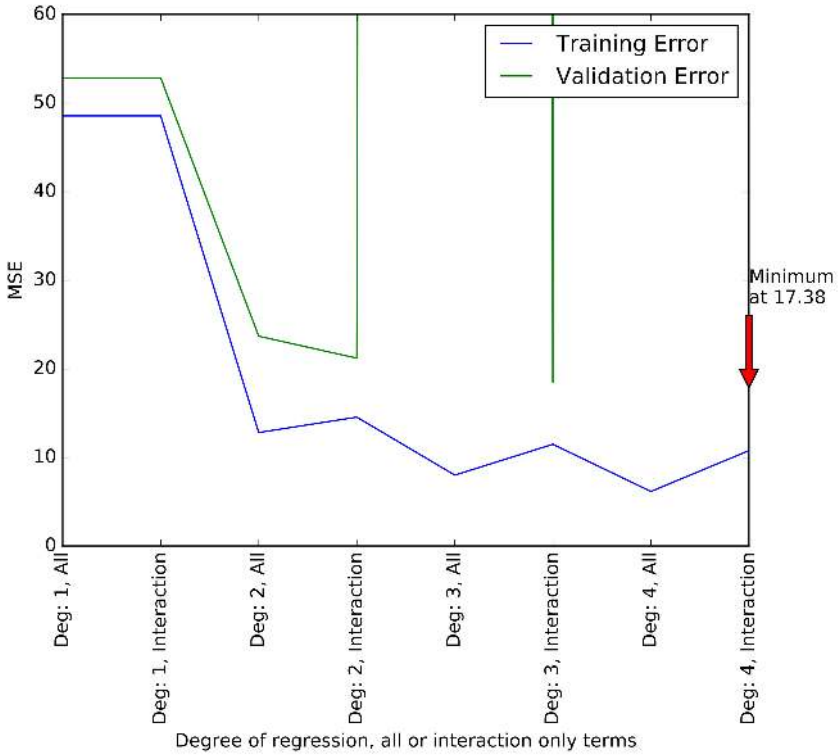

(c) Single-plane-layout, 4 sensors plus pressure. Some models are overfitting and lead to very high MSEs

Figure 5.1: Training and validation errors for all layouts over prediction algorithms. The optimal algorithm is marked with an arrow at the minimum validation error.

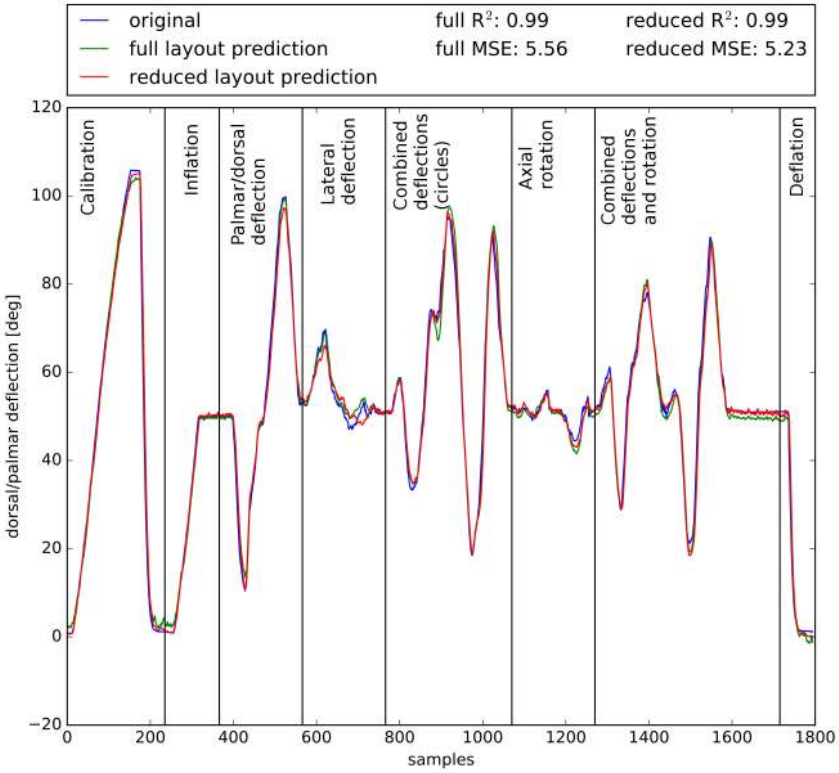

(a) Prediction of palmar/dorsal deflection.

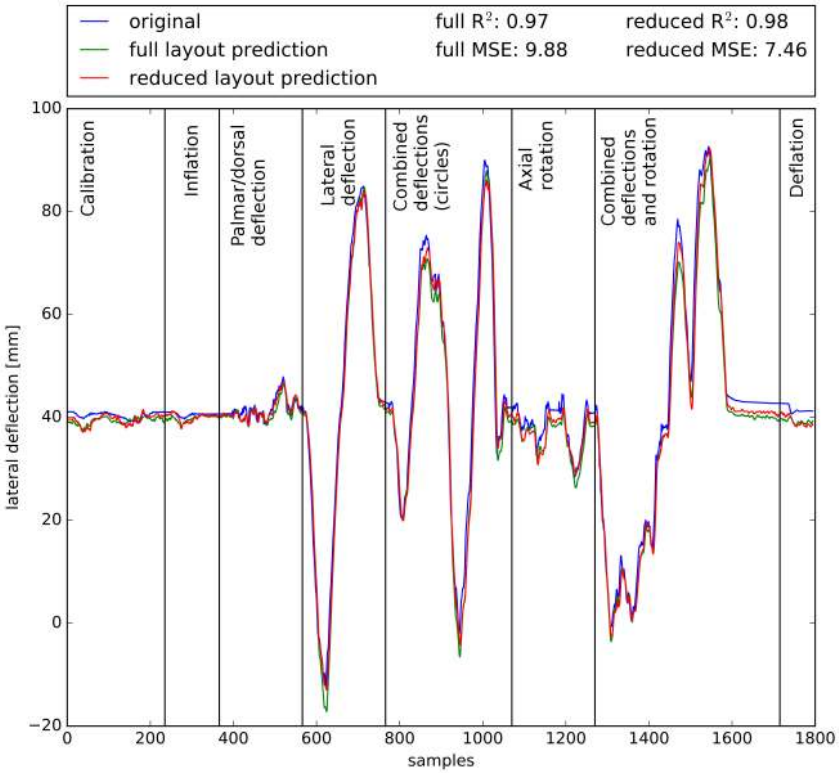

(b) Prediction of lateral deflection.

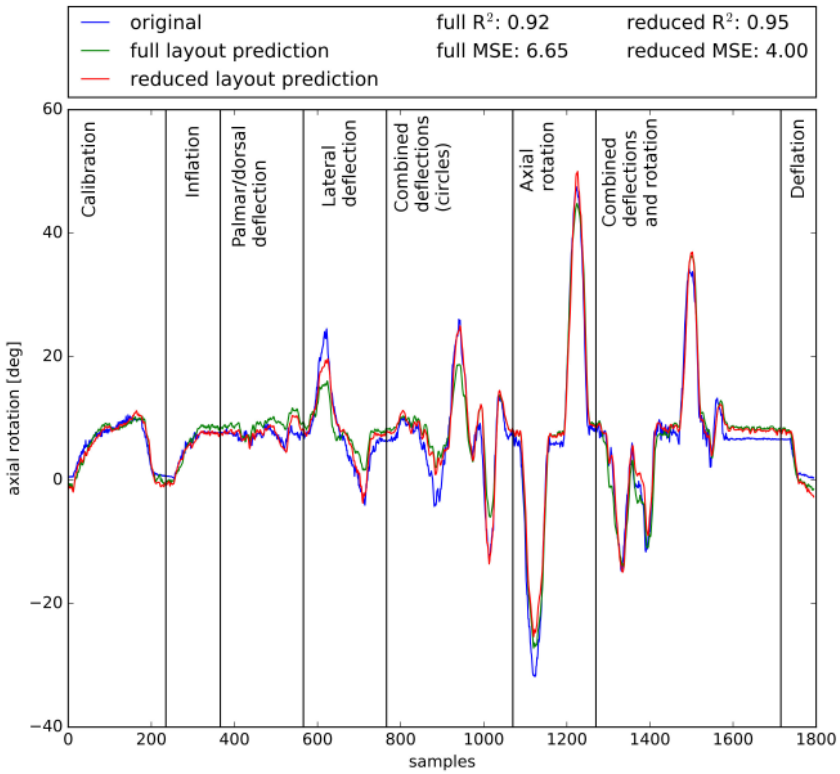

(c) Prediction of axial rotation.

Figure 5.2: Predictions of 3 deformation modes in a single step of the experiment from the full layout and the reduced layout.

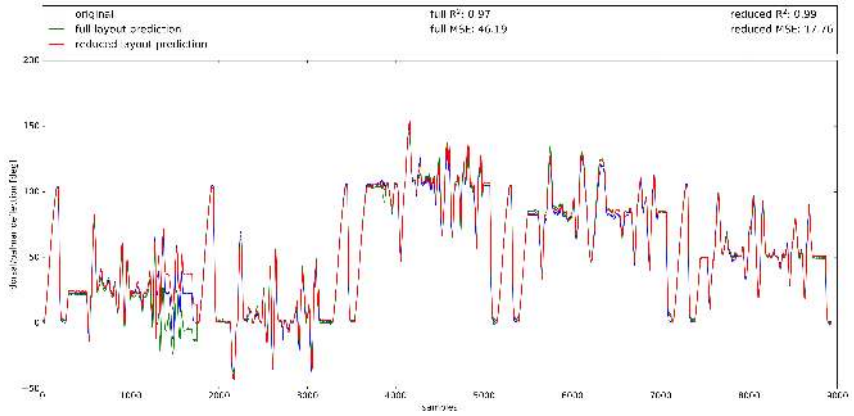

(a) Prediction of palmar/dorsal deflection.

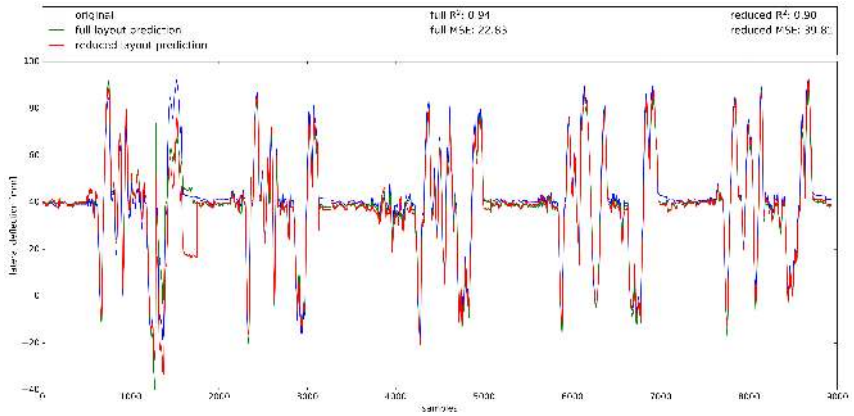

(b) Prediction of lateral deflection.

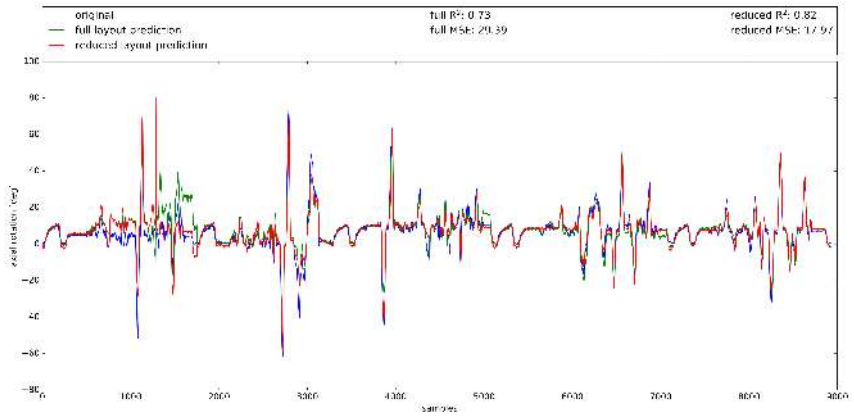

(c) Prediction of axial rotation.

Figure 5.3: Predictions of 3 deformation modes in a whole run of the experiment from the full layout and the reduced layout. The first step, until sample 2000 is predicted badly in all deformation modes, most probably due to a change of sensor contact resistance during recording.

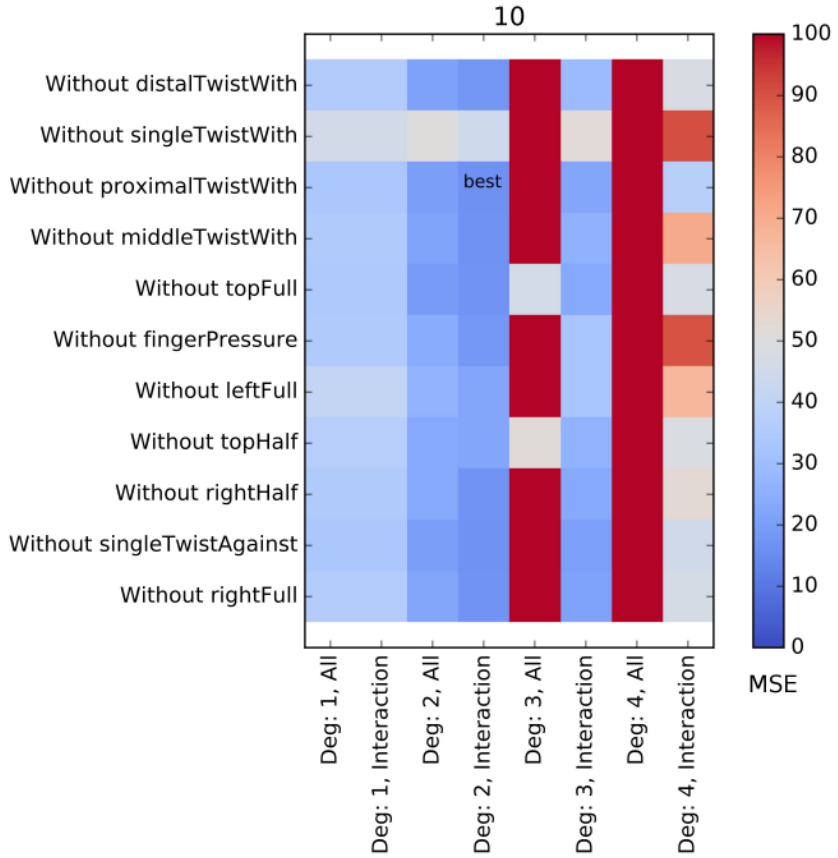

(a) Removing the proximal wrap-around twist sensor from the full layout.

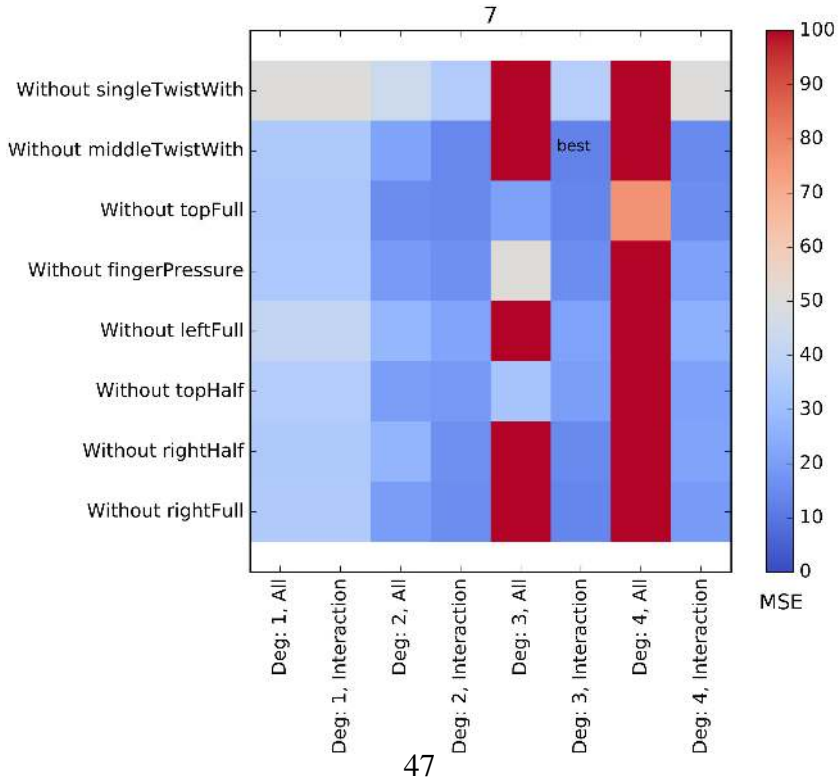

(b) Removing the middle wrap-around twist sensor.

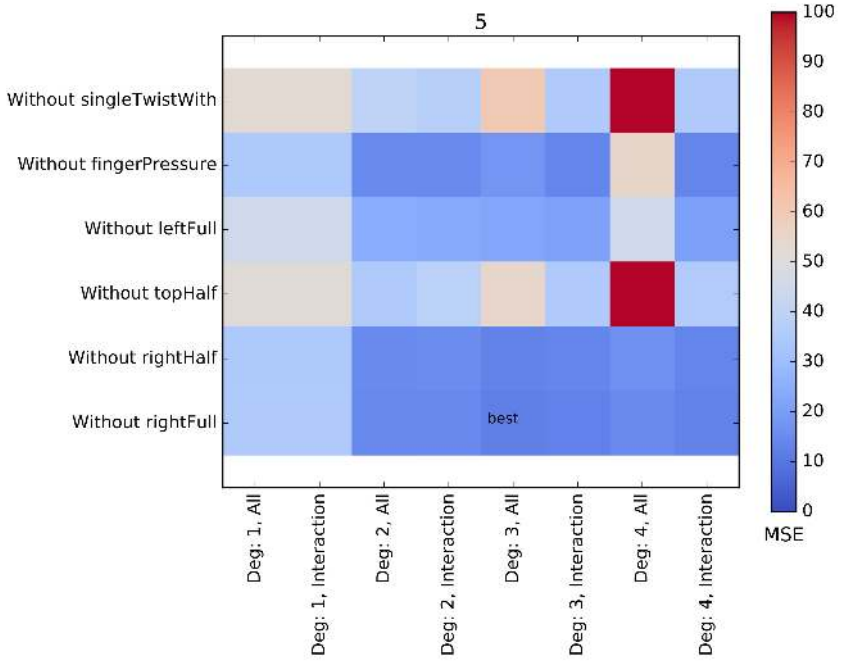

(c) Removing the lateral right full length sensor, arriving at the final layout.

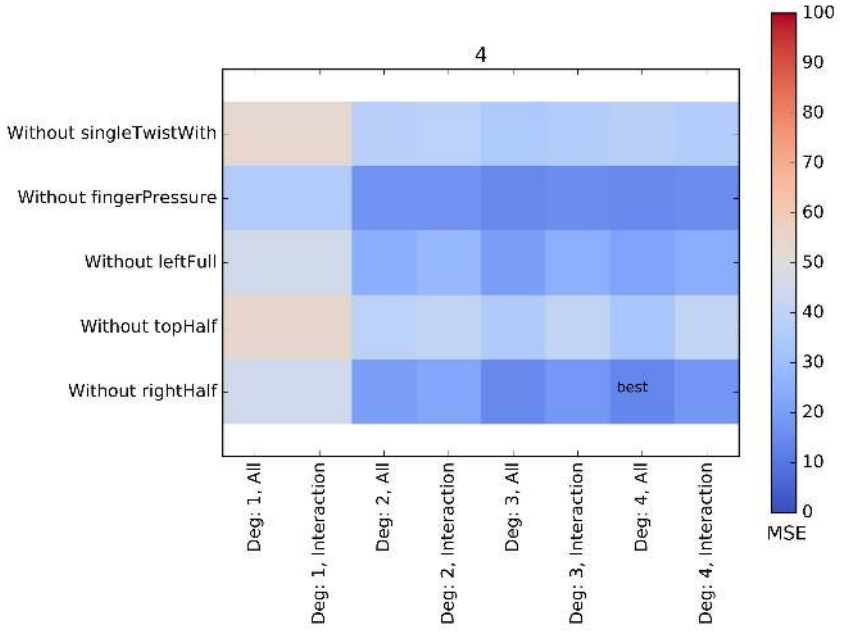

(d) Removing the lateral right half length sensor, but as seen in figure 5.5, this does not improve prediction.

Figure 5.4: sensor heatmaps

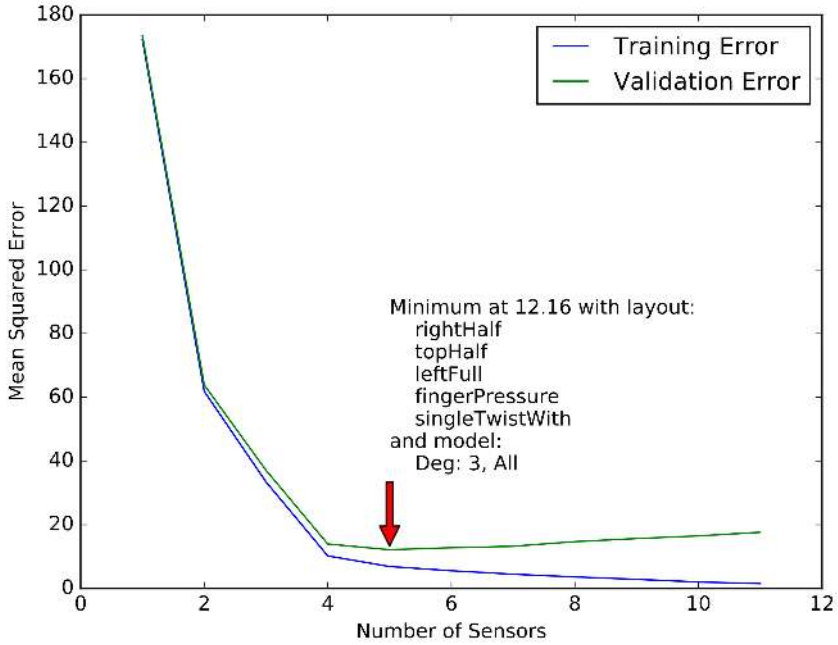

Figure 5.5: The optimal combination of sensors and prediction model is selected using the lowest validation error.

6 Limitations and Future Work

After showing that deformation modes of PneuFlex actuators can be predicted by a layout of LMSSs, I describe limitations of my method, and the produced layout and model, and give an overview on possible future work.

6.1 Limitations

As said in chapter 3, PneuFlex have a very high degree of deformation. With my layout and prediction model, detection is limited to 3 deformation modes and future experiments might show the need for additional modes. Should the need for additional modes arise, an adapted layout can be found with the method described in this thesis. Additional modes need new strain estimations, their own quantification and need to be applied, recorded and learned. Examples of additional deformation modes are the palmar contact point I did not parametrize, and the actuator buckling under very high force, which might be detectable with similar sensors.

For strain inference from very subtle deformations, strain estimations as described in this thesis might not be possible and a strain simulation might be necessary after all.

An inherent limitation of LMSSs is their loss of conductivity when pinched off, leading to invalid predictions. Although this could also be used to recognize error states like the actuator being trapped in some way. Also, while the manufacturing process of the LMSSs described by Farrow and Correll [2] does not need specialized equipment, their low resistance complicates the measuring setup.

Sadly, palmar contact was not included in the learning and reduction phases, because I did not create a parametrization of this deformation mode from the motion capturing data. Because a single conversion was able to calculate the 3 other deformation modes, I created it frist and went ahead with trying to get results showing

the method to work at all. After getting promising results, I had run out of time to work on integrating this last deformation mode and had to go ahead with the reduction phase. But as this thesis showed, it is possible to find an accurate layout of strain sensors from strain estimations. So should the need for palmar contact or new deformation modes resulting from new use cases arise, a suitable layout of strain sensors can be found based on this work.

6.2 Future Work

Future work needs to test if the benefits of shape sensing can be achieved with a PneuFlex able to predict deformation modes, like supporting grasps exploiting environmental constraints, inferring properties of grasped objects or assessing grasp quality. For this, a manipulator with sensorized PneuFlex actuators is built and used in experiments where the deformation modes were derived from. The error state recognition from pinched-off sensors proposed in the previous section could further improve this.

Other production methods of LMSSs like described by Hirsch et al. [26] could simplify production of complex sensor layouts and, by producing sensors with higher resistance, simplify the measuring setup. Their disadvantage is the need for specialized equipment.

7 Conclusion

In this thesis I introduced a method to enable sensing of prominent deformations of the PneuFlex actuator.

The PneuFlex actuator used in the RBO Hand 2 is not equipped to sense its own shape during manipulation. And while the RBO Hand 2 is already very adept in grasping, I presented research showing that by introducing shape sensing to soft actuators, their grasping performance can be improved and they are enabled to gather insight into grasped objects and their surroundings.

Observing the RBO Hand 2 at grasping tasks, I identified 4 simpler deformations, called deformation modes, of its PneuFlex actuators that, combined, describe the shape of the actuator. To motivate placement of liquid metal strain sensors (LMSSs) on the actuator, I estimated the strain induced by these deformation modes and attached sensors accordingly. To show that sensor readings can predict 3 of these deformation modes, I applied singular and combined deformation modes while recording sensor data and positional data from parts of the actuator. Regression algorithms were fit to predict deformation modes, quantified from this positional data, from sensor readings. I showed that this prediction is accurate, even after reducing the amount of LMSSs on the actuator to find an optimized layout that is easier to manufacture. Thereby, I showed that by dividing complex deformations of soft, pneumatic actuators into simpler deformation modes, strain estimations can be used to motivate informative sensor placement that allow prediction of these deformation modes, thereby giving insight into the shape of the actuator.

Should new tasks for the actuator exhibit new deformation modes or should the design of the PneuFlex actuator change, as it already did at least once [16, 4], this method can be applied again to find an informative layout of sensors to enable deformation mode prediction.

Bibliography

[1] B. S. Homberg, R. K. Katzschmann, M. R. Dogar, and D. Rus, "Haptic identification of objects using a modular soft robotic gripper," in *Intelligent Robots and Systems (IROS), 2015 IEEE/RSJ International Conference on*, Sept 2015, pp. 1698–1705.

[2] N. Farrow and N. Correll, "A soft pneumatic actuator that can sense grasp and touch," in *Intelligent Robots and Systems (IROS), 2015 IEEE/RSJ International Conference on*, Sept 2015, pp. 2317–2323.

[3] Y. L. Park, B. r. Chen, and R. J. Wood, "Soft artificial skin with multi-modal sensing capability using embedded liquid conductors," in *Sensors, 2011 IEEE*, Oct 2011, pp. 81–84.

[4] R. Deimel and O. Brock, "A novel type of compliant and underactuated robotic hand for dexterous grasping," *The International Journal of Robotics Research*, Aug. 2015. [Online]. Available: http://ijr.sagepub.com/content/early/2015/08/13/0278364915592961.abstract

[5] M. Kazemi, J.-S. Valois , J. A. D. Bagnell, and N. Pollard , "Human-inspired force compliant grasping primitives," *Autonomous Robots*, March 2014.

[6] S. Sareh, A. Jiang, A. Faragasso, Y. Noh, T. Nanayakkara, P. Dasgupta, L. D. Seneviratne, H. A. Wurdemann, and K. Althoefer, "Bio-inspired tactile sensor sleeve for surgical soft manipulators," in *2014 IEEE International Conference on Robotics and Automation (ICRA)*, May 2014, pp. 1454–1459.

[7] H. A. Wurdemann, S. Sareh, A. Shafti, Y. Noh, A. Faragasso, D. S. Chathuranga, H. Liu, S. Hirai, and K. Althoefer, "Embedded electro-conductive yarn

for shape sensing of soft robotic manipulators," in *2015 37th Annual International Conference of the IEEE Engineering in Medicine and Biology Society (EMBC)*, Aug 2015, pp. 8026–8029.

[8] E. L. White, J. C. Case, and R. K. Kramer, "Multi-element strain gauge modules for soft sensory skins," *IEEE Sensors Journal*, vol. 16, no. 8, pp. 2607–2616, April 2016.

[9] Y. L. Park, K. Chau, R. J. Black, and M. R. Cutkosky, "Force sensing robot fingers using embedded fiber bragg grating sensors and shape deposition manufacturing," in *Proceedings 2007 IEEE International Conference on Robotics and Automation*, April 2007, pp. 1510–1516.

[10] I. Oikonomidis, N. Kyriazis, and A. A. Argyros, "Efficient model-based 3d tracking of hand articulations using kinect." in *BmVC*, vol. 1, no. 2, 2011, p. 3.

[11] Y. Sun, S. Song, X. Liang, and H. Ren, "A miniature soft robotic manipulator based on novel fabrication methods," *IEEE Robotics and Automation Letters*, vol. 1, no. 2, pp. 617–623, July 2016.

[12] K. Hsiao, S. Chitta, M. Ciocarlie, and E. G. Jones, "Contact-reactive grasping of objects with partial shape information," in *Intelligent Robots and Systems (IROS), 2010 IEEE/RSJ International Conference on*, Oct 2010, pp. 1228–1235.

[13] U. Culha, S. G. Nurzaman, F. Clemens, and F. Iida, "SVAS3: Strain Vector Aided Sensorization of Soft Structures," *Sensors*, vol. 14, no. 7, pp. 12 748–12 770, Jul. 2014. [Online]. Available: http://www.mdpi.com/1424-8220/14/7/12748

[14] P. Polygerinos, Z. Wang, J. T. B. Overvelde, K. C. Galloway, R. J. Wood, K. Bertoldi, and C. J. Walsh, "Modeling of soft fiber-reinforced bending actuators," *IEEE Transactions on Robotics*, vol. 31, no. 3, pp. 778–789, June 2015.

[15] M. Bäecher, B. Hepp, F. Pece, P. G. Kry, B. Bickel, B. Thomaszewski, and O. Hilliges, "DefSense: Computational Design of Customized Deformable

Input Devices," in *SIGCHI Conference on Human Factors in Computing Systems*, ser. CHI '16. New York, NY, USA: ACM, 2016.

[16] R. Deimel and O. Brock, "A compliant hand based on a novel pneumatic actuator," in *Proceedings of the IEEE International Conference on Robotics and Automation (ICRA)*, 05 2013, pp. 01–07, http://www.robotics.tu-berlin.de/fileadmin/fg170/Publikationen_pdf/2013-icra13_Deimel_Brock.pdf. [Online]. Available: http://www.robotics.tu-berlin.de/fileadmin/fg170/Publikationen_pdf/2013-icra13_Deimel_Brock.pdf

[17] V. Wall, RBO Lab, 2016.

[18] W. Pschyrembel, O. Dornblüth, and C. Zink, *Pschyrembel klinisches Wörterbuch: Mit klinischen Syndromen und Nomina Anatomica*. De Gruyter, 1986. [Online]. Available: https://books.google.de/books?id=bY6jC5xs13gC

[19] R. Deimel, RBO Lab, 2016.

[20] C. Eppner, R. Deimel, J. Alvarez-Ruiz, M. Maertens, and O. Brock, "Exploitation of environmental constraints in human and robotic grasping," *The International Journal of Robotics Research*, vol. 34, no. 7, pp. 1021–1038, June 2015, http://www.robotics.tu-berlin.de/fileadmin/fg170/Publikationen_pdf/Eppner-Deimel-Ruiz-2015-IJRR.pdf.

[21] A. M. Dollar, L. P. Jentoft, J. H. Gao, and R. D. Howe, "Contact sensing and grasping performance of compliant hands," *Auton. Robots*, vol. 28, no. 1, pp. 65–75, Jan. 2010. [Online]. Available: http://dx.doi.org/10.1007/s10514-009-9144-9

[22] T. Feix, J. Romero, C. H. Ek, H. Schmiedmayer, and D. Kragic, "A Metric for Comparing the Anthropomorphic Motion Capability of Artificial Hands," *Robotics, IEEE Transactions on*, vol. 29, no. 1, pp. 82–93, Feb. 2013. [Online]. Available: http://grasp.xief.net

[23] P. Surmann and H. Zeyat, "Voltammetric analysis using a self-renewable non-mercury electrode," *Analytical and Bioanalytical Chemistry*, vol. 383,

no. 6, pp. 1009–1013, 2005. [Online]. Available: http://dx.doi.org/10.1007/s00216-005-0069-7

[24] *Integrated Silicon Pressure Sensor On-Chip Signal Conditioned, Temperature Compensated and Calibrated*, NXP Semiconductors, 1 2009, rev. 7. [Online]. Available: http://www.nxp.com/files/sensors/doc/data_sheet/MPX4250.pdf

[25] F. Pedregosa, G. Varoquaux, A. Gramfort, V. Michel, B. Thirion, O. Grisel, M. Blondel, P. Prettenhofer, R. Weiss, V. Dubourg, J. Vanderplas, A. Passos, D. Cournapeau, M. Brucher, M. Perrot, and E. Duchesnay, "Scikit-learn: Machine learning in Python," *Journal of Machine Learning Research*, vol. 12, pp. 2825–2830, 2011.

[26] A. Hirsch, H. O. Michaud, A. P. Gerratt, S. de Mulatier, and S. P. Lacour, "Intrinsically stretchable biphasic (solid–liquid) thin metal films," *Advanced Materials*, vol. 28, no. 22, pp. 4507–4512, 2016. [Online]. Available: http://dx.doi.org/10.1002/adma.201506234

Glossary

DAQ data acquisition. 28, 34

IR infrared light. 29

LMSS liquid metal strain sensor. 7–11, 16, 17, 24–30, 32–34, 38–40, 50–52

MSE mean squared error. 32, 38–40, 42, 43

R^2 coefficient of determination. 38, 39, 41

List of Figures